International Journal of Heat and Mass Transfer 52 (2009) 5402–5411

Contents lists available at ScienceDirect

International Journal of Heat and Mass Transfer

journal homepage: www.elsevier.com/locate/ijhmt

A numerical study of convective heat transfer from a rotating cylinder with cross-flow oscillation

J. Ghazanfarian, M.R.H. Nobari *

Mechanical Engineering Dept., Amirkabir University of Technology, 424 Hafez Avenue, Tehran-Iran, P.O. Box 15875-4413, Iran

ARTICLE INFO

Article history:
Received 6 October 2008
Received in revised form 6 May 2009
Accepted 25 June 2009
Available online 7 August 2009

Keywords:
Convective heat transfer
Finite element
Arbitrary Lagrangian–Eulerian
CBS method
Rotating cylinder
Cross-flow oscillation

ABSTRACT

This article presents a numerical investigation of convective heat transfer from a rotating cylinder with cross-flow oscillation. A finite element analysis using Characteristic Based Split method (CBS) is developed to solve governing equations involving continuity, Navier–Stokes, and energy equations. Dynamic unstructured triangular grid is used employing improved lineal and torsional spring analogy which is coupled with the solver by the Arbitrary Lagrangian–Eulerian (ALE) formulation. After verifying the numerical code accuracy, simulations are conducted to study convective heat transfer past a rotating cylinder with cross-flow oscillation at Reynolds numbers of 50, 100, and 200. Different rotational speeds of the cylinder normalized by free stream velocity, in the range of 0–2.5 are considered at various oscillating amplitudes and frequencies and three different Prandtl numbers of 0.7, 6, and 20. Effects of oscillation and rotation of cylinder on the temperature and flow field, vortex lock-on, mean Nusselt number, and the pattern of vortex shedding are investigated in detail considering iso-temperature and iso-flux boundary conditions on the cylinder surface. It is found that similar to the fixed cylinder, beyond a critical rotating speed, vortex shedding is mainly suppressed. Also by increasing the non-dimensional rotational speed of the cylinder, both the Nusselt number and the drag coefficient decrease rapidly. However, in vortex lock-on region, the Nusselt number increases in a large amount.

1. Introduction

The flow and heat transfer around a circular cylinder have been studied mainly due to the importance of vortex induced vibration (VIV) phenomenon especially in the fields such as off-shore and civil engineering, heat exchanger design, nuclear reactor fuel rod, and steel cable of suspension bridge.

Various studies have been carried out for a flow over an oscillating cylinder using experimental numerical tools. Gerrard [1] studied vortex shedding mechanisms and presented a model to describe the phenomenon. The study by Koopman [2] has investigated the effect of cross-flow oscillation of a cylinder on the vortex shedding frequency and determined the lock-on region where the shedding frequency coincides with the oscillating frequency at low Reynolds numbers. Griffin and Ramberg [3] studied the effect of longitudinal oscillation of a cylinder on the vortex shedding including lock-on phenomenon. By using visualization techniques, they have also observed that the longitudinal spacing of the vortices have an inverse relation with the oscillation frequency. Williamson and Roshko [4] have investigated the effect of amplitude of oscillation on the wake formation. They declared that by increasing the amplitude of oscillation, vortex shedding pattern develops as a pair of vortices on one side (2S) and a single vortex on the other side (P + S). Hall and Griffin [5] simulated the oscillatory flow around a fixed cylinder by applying a sinusoidal horizontal velocity component on the incoming flow to investigate the occurrence of lock-on. The study by Nobari and Naderan [6] has investigated the flow pattern around cross-flow and inline oscillating cylinder, where the effects of inline and cross-flow oscillation on the drag coefficient, flow field, occurrence of lock-on, and wake pattern are discussed in detail. Moreover, flow past a circular cylinder with a rotary oscillation has been investigated experimentally by Filler et al. [7] and numerically by Baek and Sung [8].

Forced convection from a heated cylinder with rotational oscillation placed in a uniform stream was investigated by Mahfouz and Badr [9]. In their study the lock-on phenomenon was detected and its effect on the thermal field was determined. Their results indicate that the lock-on phenomenon occurs within a band of frequency near the natural frequency and the heat transfer coefficient increases significantly in the lock-on frequency range. Fu and Tong [10] numerically studied the flow structures and heat transfer characteristics of a heated cylinder oscillating transversely. They showed that the interaction between the oscillating cylinder and the vortex shedding dominates the state of the wake and the flow and the thermal fields may approach a periodic state in the lock-on regime at which the heat transfer is enhanced remarkably. As an internal flow over an immersed oscillating body, a numerical

---

* Corresponding author. Fax: +98 2166419736.
E-mail address: mrnobari@cic.aut.ac.ir (M.R.H. Nobari).

0017-9310/$ - see front matter © 2009 Elsevier Ltd. All rights reserved.
doi:10.1016/j.ijheatmasstransfer.2009.06.036

Nomenclature

A	non-dimensional amplitude
C	Courant number
C_D	drag coefficient
C_L	lift coefficient
$\mathbf{C}_u$	convective matrix
c	fluid velocity relative to mesh
F	non-dimensional frequency
$\mathbf{f}$	force vector
f	frequency
$\mathbf{f}^s$	stabilizing vector
f_s	Strouhal frequency
h	element size
K_u	stabilizing coefficient
K_τ	diffusion matrix
k	diffusion coefficient
$\mathbf{M}$	mass matrix
N	shape function
n	time step number
p	pressure
Q	source term
Re	Reynolds number
St	Strouhal number
t	time
U	velocity components
x	coordinate, amplitude
x'	transformed coordinate
Greeks	
α	rotational velocity
δ	infinitesimal displacement
θ	implicit or explicit parameter
ν	kinematic viscosity
ϕ	scalar variable
ψ	grid velocity component
Superscripts	
–	average
*	intermediate velocity
Subscript	
ijk	

simulation was performed by Fu and Tong [11] to study the influence on the heat transfer rate from heated walls in a channel with an oscillating cylinder. They found that the position and the diameter of the cylinder affect significantly on the flow and thermal fields in the channel flow.

Many attempts have been made for controlling the wake behind a circular cylinder in recent years, especially for the purpose of suppressing vortex shedding using passive and active controls. The effects of the rotation of a cylinder on a laminar flow have been investigated by Kang et al. [12] in the fully developed stage involving vortex shedding at $47 < Re < 200$. The rotation of a cylinder in a viscous uniform flow is expected to modify wake flow pattern and vortex shedding configuration which may reduce flow-induced oscillation or augment the lift force. Ingham and Tang [13] numerically investigated the rotating cylinder flow $Re < 47$ at relatively small non-dimensional rotational speeds ($\alpha < 3$). They found that although the vortex shedding does not occur in the wake region, the rotation delays and inhibits the boundary-layer separation. The study by Badr et al. [14] numerically investigated unsteady flow at $Re = 50$, 100, and 200, focusing on the flow pattern during an early time period after the impulsive rotation and translation of a cylinder. Tang and Ingham [15] have examined steady flow at $Re = 50$ and 100 in the rotational speed range of $0 < \alpha < 1$ by solving time-independent governing equations and have presented the changes in the flow variables.

However, so far there is no study on the heat transfer characteristics of the flow past a rotating cylinder with cross-flow oscillation. This is the main concern of the present paper. Here, the effects of rotation of the cylinder with cross-flow oscillation on the heat transfer are studied in detail. The two dimensional governing equations are solved on a moving unstructured mesh using a finite element method based on the CBS algorithm coupled by ALE formulation. Simulations are conducted at moderate Reynolds numbers of 100, 200, and 300 considering two different thermal boundary conditions of iso-temperature and iso-flux on the cylinder surface. Effects of different non-dimensional physical parameters consisting of Reynolds number, Strouhal number, rotating speed (α), Nusselt number, Prandtl number, oscillating amplitude and frequency on the heat transfer are investigated in both lock-on and non-lock-on regions.

2. Governing equations

Here two-dimensional incompressible viscous flow over a rotational cylinder with cross-flow oscillation is considered to study the heat transfer from either iso-temperature or iso-flux cylinder surface. The governing equations consisting of continuity, momentum, and energy equations can be written in the concise form as

$$\frac{\partial U_i}{\partial x_i} = 0, \tag{1}$$

$$\frac{\partial U_i}{\partial t} + u_j \frac{\partial U_i}{\partial x_j} = -\frac{\partial p}{\partial x_i} + \nu \frac{\partial^2 U_i}{\partial x_j \partial x_j}, \tag{2}$$

$$\frac{\partial T}{\partial t} + u_j \frac{\partial T}{\partial x_j} = \frac{k}{\rho C_p} \frac{\partial^2 T}{\partial x_j \partial x_j}, \tag{3}$$

where U_i denotes the velocity components, p the pressure, ν the kinematic viscosity, T the temperature, k the conductivity, and C_p the specific heat capacity.

In this study Eqs. (1)–(3) are solved in a deforming boundary domain. Consequently, the ALE formulation [16,17] is used as follows:

$$\frac{\partial U_i}{\partial t} + c_j \frac{\partial U_i}{\partial x_j} = -\frac{\partial p}{\partial x_i} + \nu \frac{\partial^2 U_i}{\partial x_j \partial x_j}, \tag{4}$$

$$\frac{\partial T}{\partial t} + c_j \frac{\partial T}{\partial x_j} = \frac{k}{\rho C_p} \frac{\partial^2 T}{\partial x_j \partial x_j}, \tag{5}$$

where $c_i = u_i - \psi_i$ is the fluid velocity relative to the coordinates attached to the grid. Hence, ψ_i denotes the grid velocity components. It is easy to observe that Eqs. (4) and (5) become a Lagrangian equation when the grid velocity, ψ_i, equals to the fluid velocity, u_i, and becomes an Eulerian equation when $\psi_i = 0$.

Dynamic fluid grids are used for the solution of the flow with moving boundaries employing the arbitrary motion of two-dimensional dynamic unstructured fluid grids controlled by both linear and torsional springs to protect the grid against the deformation causing instabilities in the numerical solution. More details of the method can be bound in the study carried out by Farhat et al. [18].

The governing equations are solved by a characteristic based split (CBS) finite element method in which the splitting procedure follows the algorithm initially introduced by Chorin [19] for incompressible flow problems in the finite difference context. A similar extension of the split to the finite element formulation has been carried out for the first time by Zienkiewicz and Codina [20], which provides a fully explicit algorithm for incompressible flows. A C++ computer code is used to solve the governing equations on a dynamic unstructured two-dimensional grid.

3. Numerical scheme

To split along the characteristics, a typical scalar convection–diffusion equation is considered as

$$\frac{\partial\phi}{\partial t}+U\frac{\partial\phi}{\partial x}-\frac{\partial}{\partial x}\left(k\frac{\partial\phi}{\partial x}\right)+Q=0, \tag{6}$$

where U is the convective velocity. Since Eq. (6) is not self-adjoint, therefore, the result of standard Galerkin formulation is not optimal. To deal with this problem, a new independent variable is introduced as $dx' = dx - U\,dt$ which transforms the convection–diffusion equation to the following self-adjoint form:

$$\frac{\partial\phi}{\partial t}-\frac{\partial}{\partial x'}\left(k\frac{\partial\phi}{\partial x'}\right)+Q(x')=0, \tag{7}$$

where the convective acceleration term disappears and it enables the optimum results to be obtained using the standard Galerkin approximation in Eq. (7). In one-dimensional case with no conduction or source term, $k = 0$ and $Q = 0$, the solution of Eq. (7) results in $\phi(x) = \phi(x - Ut) =$ constant assuming constant U velocity. This is a typical equation of a wave propagation even if the conduction or source term is not zero. The time discretization of Eq. (7) along the characteristics can be written as

$$\frac{1}{\Delta t}\left(\phi^{n+1}-\phi^{n}|_{(x-\delta)}\right)\approx\theta\left[\frac{\partial}{\partial x}\left(k\frac{\partial\phi}{\partial x}\right)-Q\right]^{n+1}+(1-\theta)\left[\frac{\partial}{\partial x}\left(k\frac{\partial\phi}{\partial x}\right)-Q\right]^{n}_{(x-\delta)}, \tag{8}$$

where θ is zero in fully explicit case and between zero and unity in the semi- and fully implicit cases, respectively. To avoid difficulties due to mesh updating in moving coordinates, the alternative form can be considered using Taylor expansion.

$$\phi^{n}|^{(x-\delta)}\approx\phi^{n}-\delta\frac{\partial\phi^{n}}{\partial x}+O(\Delta x^{2}). \tag{9}$$

Assuming $\theta = 0.5$

$$\frac{1}{2}\frac{\partial}{\partial x}\left(k\frac{\partial\phi}{\partial x}\right)^{n}_{(x-\delta)}\approx\frac{1}{2}\frac{\partial}{\partial x}\left(k\frac{\partial\phi}{\partial x}\right)^{n}-\frac{\delta}{2}\frac{\partial}{\partial x}\left[\frac{\partial}{\partial x}\left(k\frac{\partial\phi}{\partial x}\right)^{n}\right]+O(\Delta t^{2}), \tag{10}$$

$$\frac{1}{2}Q|_{(x-\delta)}\approx\frac{Q^{n}}{2}-\frac{\delta}{2}\frac{\partial Q^{n}}{\partial x}, \tag{11}$$

where $\delta = \overline{U}\Delta t$ is the distance traveled by the fluid particle in x direction and $\overline{U}$ is the average value of U along the characteristics as shown in Fig. 1. Different approximations of $\overline{U}$ lead to different stabilizing terms. The most common choice for the average velocity, which is also used in this paper, is introduced by Zienkiewicz and Codina [20,21].

$$\overline{U}=\frac{1}{2}\left(U^{n+1}+U^{n}|_{(x-\delta)}\right). \tag{12}$$

Using Taylor expansion to substitute Eq. (12) into Eq. (8) and neglecting higher order derivatives considering $\theta = 0.5$, the following equation can be obtained:

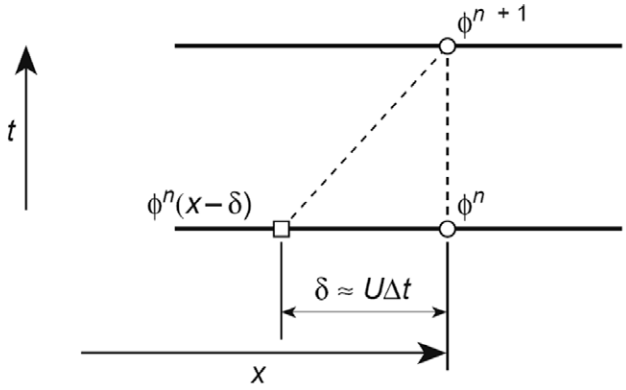

Fig. 1. One-dimensional characteristic-Galerkin method.

$$\begin{aligned}\frac{1}{\Delta t}(\phi^{n+1}-\phi^{n})={}&-U^{n+1/2}\frac{\partial\phi^{n}}{\partial x}+\frac{\Delta t}{2}U^{n}\frac{\partial U^{n}}{\partial x}\frac{\partial\phi^{n}}{\partial x}\\&+\frac{\Delta t}{2}U^{n+1/2}U^{n+1/2}\frac{\partial^{2}\phi}{\partial x^{2}}+\frac{\partial}{\partial x}\left(k\frac{\partial\phi}{\partial x}\right)^{n+1/2}\\&-\frac{\Delta t}{2}U^{n+1/2}\frac{\partial}{\partial x}\left[\frac{\partial}{\partial x}\left(k\frac{\partial\phi}{\partial x}\right)^{n}\right]-Q+\frac{\Delta t}{2}U^{n+1/2}\frac{\partial Q}{\partial x},\end{aligned} \tag{13}$$

where $n+\frac{1}{2}$ terms are approximated by n to get the fully explicit version of the algorithm.

The final form of the explicit discretization of the multi-dimensional convection–diffusion equation in indicial conservative form can be written as

$$\begin{aligned}\Delta\phi=\phi^{n+1}-\phi^{n}={}&-\Delta t\left[\frac{(\partial U_{j}\phi)}{\partial x_{j}}-\frac{\partial}{\partial x_{i}}\left(k\frac{\partial\phi}{\partial x_{i}}\right)+Q\right]^{n}\\&+\frac{\Delta t^{2}}{2}U_{k}^{n}\frac{\partial}{\partial x_{k}}\left[\frac{\partial(U_{j}\phi)}{\partial x_{j}}-\frac{\partial}{\partial x_{i}}\left(k\frac{\partial\phi}{\partial x_{i}}\right)+Q\right]^{n}.\end{aligned} \tag{14}$$

Since a fully explicit solution needs no iterative process, in practice fully explicit form is much easier to handle. The CBS algorithm for the solution of Navier–Stokes equations is expressed in the following order:

1. Solution of momentum equation eliminating pressure term (Eq. (15)).
2. Calculation of pressure from Poisson equation (Eq. (17)).
3. Correction of velocities (Eq. (16)).
4. Calculation of energy equation or any other scalar equation.

In the first step, a new auxiliary velocity $\mathbf{U}^{*}$ is defined as

$$U_{i}^{*}-U_{i}^{n}=\Delta t\left[-u_{j}\frac{\partial U_{i}}{\partial x_{j}}+\nu\frac{\partial^{2}U_{i}}{\partial x_{j}\partial x_{j}}\right]^{n}+\frac{\Delta t^{2}}{2}u_{k}\frac{\partial}{\partial x_{k}}\left[u_{j}\frac{\partial U_{i}}{\partial x_{j}}\right]^{n}. \tag{15}$$

This represents the first part of the split procedure. To determine the pressure value over the entire solution domain, the velocities are corrected as

$$U_{i}^{n+1}-U_{i}^{*}=-\Delta t\frac{\partial p^{n}}{\partial x_{i}}-\frac{\Delta t^{2}}{2}u_{k}\frac{\partial^{2}p^{n+1}}{\partial x_{k}\partial x_{i}}. \tag{16}$$

The solution of this equation is the third step of CBS algorithm where the pressure is considered as a known quantity, but it is corrected in the second step. Taking divergence of both sides of Eq. (16) and using continuity equation, Eq. (16) changes into the Poisson equation for the pressure field.

$$\Delta t\frac{\partial^{2}p^{n+1}}{\partial x_{i}\partial x_{i}}=\frac{\partial U_{i}^{*}}{\partial x_{i}}. \tag{17}$$

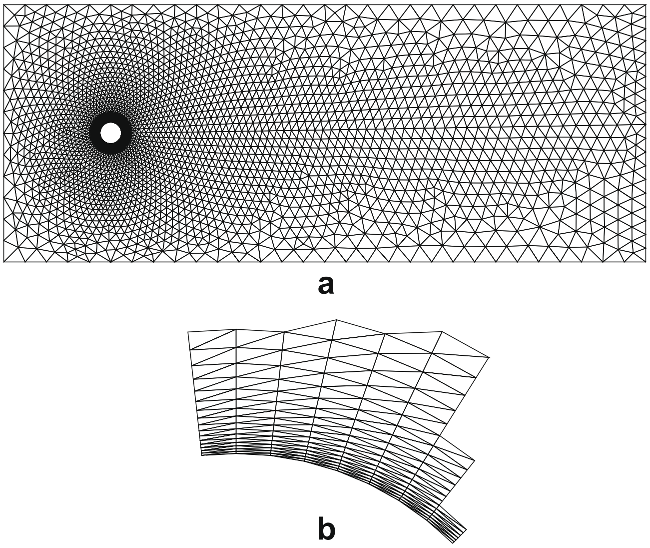

Fig. 2. Numerical grid used to simulate flow over the rotating cylinder with cross-flow oscillation, (a) entire domain with 3945 nodes and 7798 elements (b) grid close up and boundary-layer elements in the vicinity of cylinder.

Finally, the discretized form of energy equation can be expressed as

$$T^* - T^n = \Delta t\left[-u_j\frac{\partial T}{\partial x_j} + \nu\frac{\partial^2 T}{\partial x_j \partial x_j}\right]^n + \frac{\Delta t^2}{2}u_k\frac{\partial}{\partial x_k}\left[u_j\frac{\partial T}{\partial x_j}\right]^n. \tag{18}$$

At this stage all the flow field variables are known in the new time step of $n+1$. Now the derived equations may be solved by standard Galerkin finite element procedure. To do so, the computational domain is discretized into linear triangular elements. In CBS method, it is possible to use the same degree of shape functions for pressure and velocity approximations without having any numerical oscillations in the pressure field [22]. More detail of discretization is available in Appendix A.

It is obvious that the CBS algorithm in the explicit form is only conditionally stable. To determine the time step size of the solution, two stability conditions exist. The first one is concerned with the convective terms and is given as the CFL condition.

$$\Delta t = C\frac{h}{|u|}, \tag{19}$$

where $0 < C < 1$ is the Courant number $(\Delta t u/h)$ in which h is the element size. The second stability condition is due to diffusion and can be expressed as

$$\Delta t \leqslant \frac{h^2}{4k}. \tag{20}$$

To avoid small time step sizes due to the existence of boundary-layer elements, diffusion terms are computed implicitly and consequently the second stability condition may be ignored.

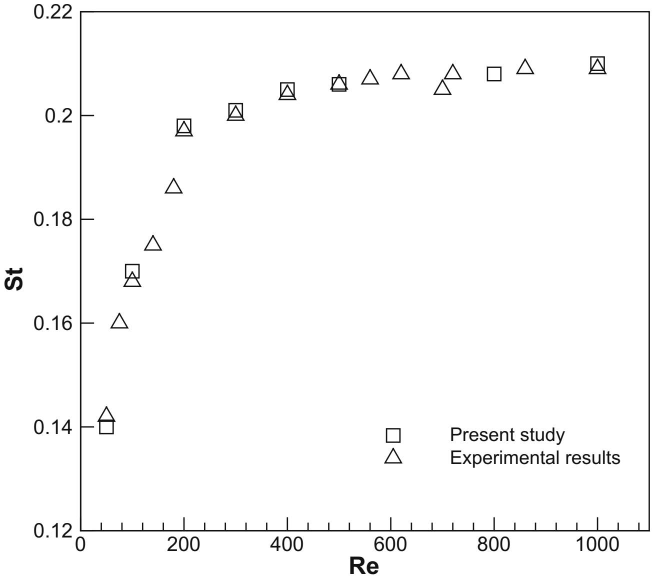

Fig. 3. Variation of *St* vs *Re* for fixed cylinder compared with the experimental results [23].

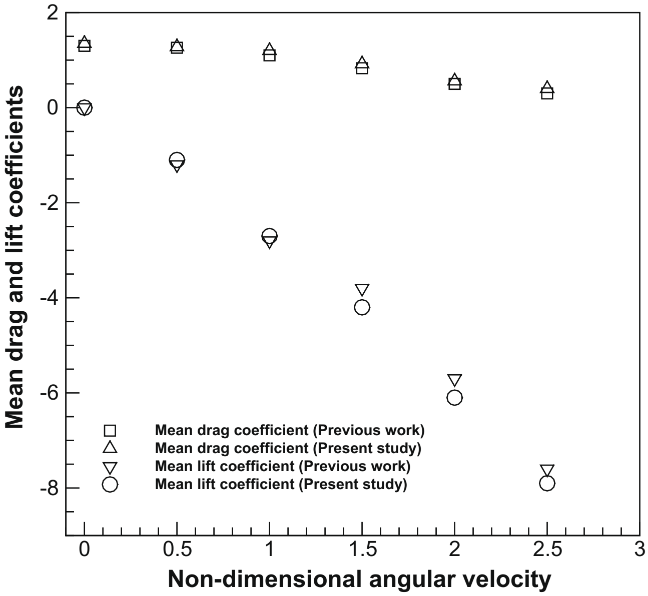

Fig. 4. Mean lift and drag coefficients vs non-dimensional rotational speed (α) for rotating fixed cylinder at $Re = 100$ comparing with previous work [12].

The geometry of the problem and the grids used in the numerical solution are shown in Fig. 2. No slip boundary condition is

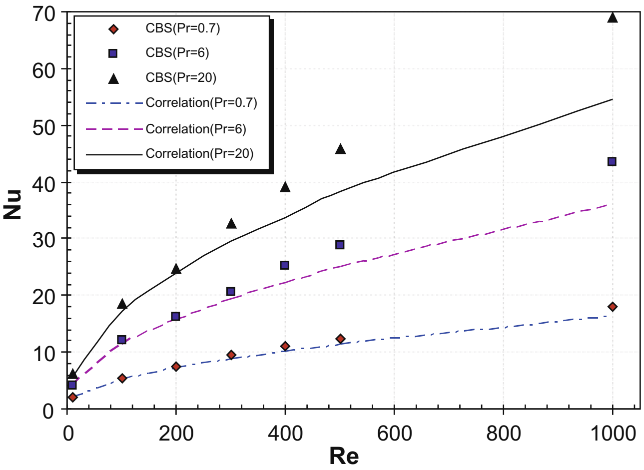

Fig. 5. Comparison of average Nusselt number of fixed cylinder with experimental results [24] at different values of *Re* and *Pr*.

Table 1
Non-dimensional frequencies and amplitudes used for cross-flow oscillating cylinder.

Non-dimensional amplitude (*A*)	0.2, 0.4, 0.6
Non-dimensional frequency (*F*)	0.6, 0.8, 1, 1.3

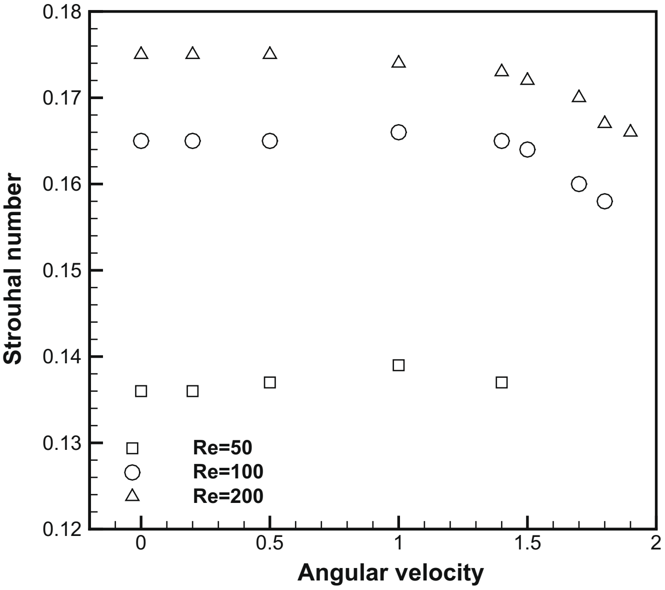

Fig. 6. Variation of Strouhal number vs. non-dimensional rotational speed for various *Re* numbers from present study and from Ref. [12].

applied on the cylinder and at the inlet and at the two horizontal boundaries away from the cylinder, the velocity is considered as the free stream velocity. At the outflow, the free boundary condition is applied, which is equivalent to extending the validity of weak form of the governing equations to the outflow. For the pressure, Neumann boundary conditions are used at all the boundaries except at the outlet where the constant pressure is applied. To study the heat transfer form a rotating cylinder with cross-flow oscillation, two different thermal boundaries consisting of iso-temperature and iso-heat flux at the cylinder are taken into account. Also, the initial conditions for the velocity and the temperature are considered as zero.

4. Numerical code accuracy

The accuracy of the numerical code developed here is tested by comparing the numerical results obtained with the experimental data available considering various aspects. The first case deals with the verification of the variation of Strouhal number with respect to the Reynolds number for the fixed non-rotating cylinder. As shown in Fig. 3, there is a good agreement between the experimental data and the current computational results. In the second case a flow past a rotating cylinder is simulated, and the drag and lift coefficients are compared with the previous work in Fig. 4. As is evident from the figure, the present computed results indicate a very good agreement with the previous work [12], where the maximum error is 6%.

To evaluate the performance of energy equation solution, the variation of average Nusselt number of the fixed cylinder is compared with the experimental results [24] at a wide range of *Re* and *Pr* in Fig. 5. It is obvious that above $Re = 300$, due to the three

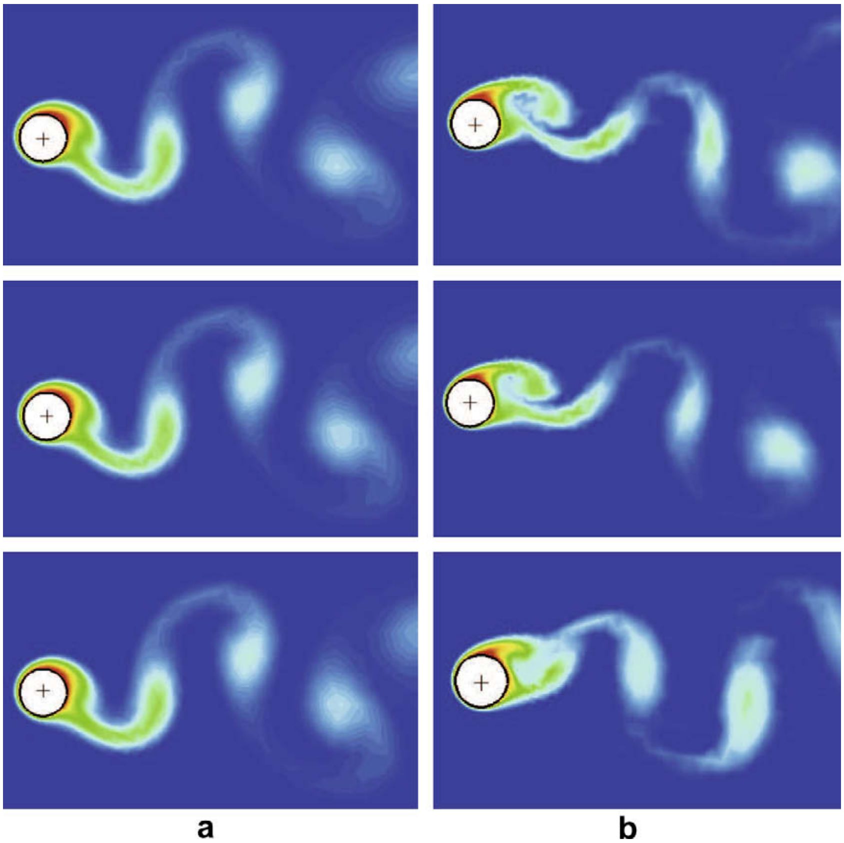

Fig. 7. Temperature field of rotating cylinder with cross-flow oscillation at the beginning of three consecutive cycles when $Re = 100$, $\alpha = 0.5$, and $A = 0.2$, (a) $F = 1$, (b) $F = 0.6$.

dimensionality of the nature of problem, the predicted results of the written code deviate from the experimental results but below that a reliable agreement can be observed.

5. Results and discussion

In this section, the numerical results obtained for the convective heat transfer from an incompressible flow over a rotating cylinder with cross flow oscillations are investigated considering two different thermal boundary conditions on the cylinder surface involving the iso-temperature and iso-flux.

The oscillatory motion of the cylinder is simulated as

$$x = \text{constant},\quad y = Y\sin(2\pi ft), \tag{21}$$

where, Y and f are amplitude and frequency of oscillation, respectively. Values of non-dimensional amplitudes ($A = Y/d$) and non-dimensional frequencies ($F = f/f_s$) used for the cross-flow oscillations of the cylinder are listed in Table 1 where f_s is the Strouhal frequency. Variation of the Strouhal number with respect to the rotational speed (α) and the comparison with the data from [12] is shown in Fig. 6. From this figure it is obvious that the rotation of the cylinder does not significantly affect on the Strouhal number.

Visualization of the vorticity and the temperature field in the flow over a rotating cylinder with cross-flow oscillation helps understand different physical phenomena taking place in the flow field such as vortex shedding and the corresponding lock-on status. Hence the temperature field at $Re = 100$, $\alpha = 0.5$, and $A = 0.2$ are shown in Fig. 7 at the beginning of three consecutive cycles for two different oscillation amplitudes. The shedding vortices in this figure appear as the lumps of heated fluid convected away from the cylinder. The left column in Fig. 7 ($F = 1$) is concerned with the lock-on phenomenon and the right column ($F = 0.6$) is associated with the non-locked-on case. Due to lock-on phenomenon, the vortex patterns in the left column of Fig. 7 are similar to each other resulting from the vortex shedding synchronization with the cylinder motion.

Figs. 8 and 9 show the vorticity and the temperature fields along with the streamlines corresponding to $\alpha = 0.5$ and 1.5 at four different times of a complete cycle for $Re = 100$, $A = 0.2$, and $F = 1$. The mechanism of the heat diffusion moving downstream is clearly shown in these figures where the fluid contained within each vortex gets cooler as it moves away from the cylinder. It is clearly shown that the vortex shedding developing at $\alpha = 0$ also occurs at the low values of non-dimensional rotational speed. Critical value of α beyond which the vortex shedding is mainly suppressed is equal to 2 at $Re = 100$. For $\alpha < \alpha_{critical}$, rotational effects are confined to the region near the cylinder surface. By increasing α, the negative vorticity on the upper side of the cylinder becomes more dominant than the positive vorticity on the lower side. This makes the vortices to go upper in the flow field and strengthens the upper vortex.

It can be also observed that the Nu distribution at the middle of the cycle is a mirror image of that at the end of it, which explains the asymmetry of the thermal field every half cycle. This phenomenon can be ascertained by comparing the isothermal patterns at the beginning and at the half of the oscillation cycle in Figs. 8–10.

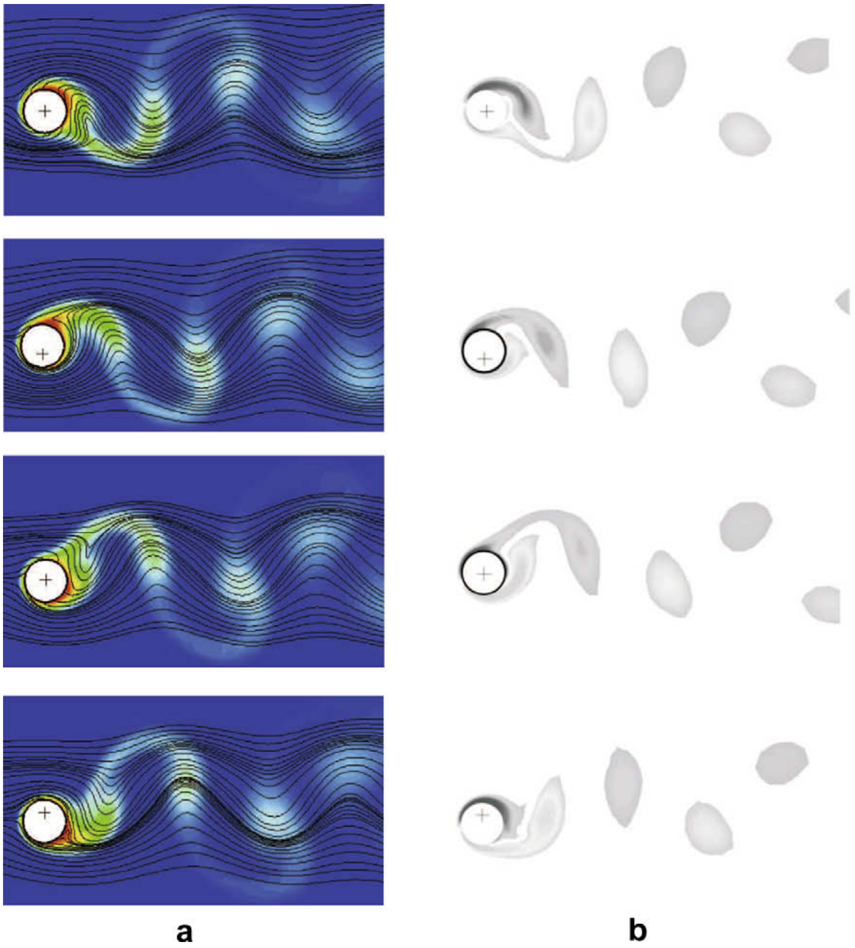

Fig. 8. (a) Temperature field and streamlines, (b) vorticity field for cross-flow oscillating cylinder with rotation at $Re = 100$, $A = 0.2$, $F = 1$, and $\alpha = 0.5$.

Subsequently, as shown in the right column of Fig. 10, for $\alpha > \alpha_{critical}$ the flow has two vorticity bubbles attached to the cylinder and the vortex shedding is suppressed to only one vortex which sheds in the third quarter of the cycle. As α increases further, the bubbles become more thinner and more inclined in the direction of rotation.

After studying different aspects of the vorticity and temperature field, now the characteristics of the mean Nusselt number and drag forces exerted on the rotating cylinder with cross-flow oscillation is investigated. Here the Nusselt number and the lift and drag coefficients are averaged based on the cycle time and along the cylinder surface. Variations of the Nusselt number and drag coefficients at various combinations of non-dimensional rotational speeds, Reynolds numbers, and amplitude and frequency of oscillations are shown in Figs. 11–13. The Nusselt number is defined as

$$Nu_T = -\frac{\partial T_s}{\partial n}, \tag{22}$$

where T_s is the surface temperature and n is the unit vector normal to the boundary. Although process of vortex shedding depends on the amplitude and frequency oscillation, it has a direct effect on the heat convection resulting from the amount of the heat carried by each vortex. The shedding frequency and the size of the vortices are both important factors influencing on the heat convection process. Fig. 11 shows the variation of the Nusselt number with respect to the non-dimensional rotational speed of the cylinder at the various Reynolds numbers and amplitudes of oscillation. Frequency of oscillation is chosen in such a way that the lock-on condition occurs. It is observed that by increasing the Reynolds number in a trend similar to the fixed cylinder, the Nusselt number increases. As α increases due to the vortex shedding suppression and the thicker thermal boundary-layer, the mean Nusselt number decreases (Fig. 11). As is evident from Fig. 11, by increasing the amplitude of oscillation the relative velocity of the cylinder increases, causing the Nusselt number to increase.

The behavior of the Nusselt number in the lock-on region is further investigated in Fig. 12 where the fixed rotating case also included. In this figure the Nusselt number is depicted at two frequencies of oscillation which are lower and higher than the Strouhal frequency. At the frequency below the Strouhal frequency ($F = 0.6$ in the figure), the Nusselt number is nearly the same as the fixed cylinder and the slight increase is due to the higher velocity of the fluid in the vicinity of the cylinder. As the frequency of oscillation increases up to the lock-on occurrence ($F = 1$ in the figure), the Nusselt number increases indicating heat transfer augmentation. The major part of the Nusselt number increment originates from the vortex synchronization phenomenon. Similar trends as explained in Fig. 11 can be observed in this figure.

As a sample result, the mean drag coefficient with respect to the non-dimensional rotational speed of the cylinder is shown in Fig. 13 at various Reynolds numbers and amplitudes of oscillation in lock-on region. It is seen that by increasing Reynolds number in a trend similar to the fixed cylinder, the drag coefficient decreases. Furthermore, in the case of rotating cylinder, the friction drag is of the same order of magnitude as the pressure drag. By increasing α, the relative velocity of the cylinder (friction drag) increases with the decrease in the pressure drag, resulting in the reduction of the total drag.

The behavior of drag coefficient is similar to the Nusselt number which is explained in Fig. 12 where the drag coefficient is depicted at two frequencies of oscillation which are less and higher than the Strouhal frequency. This figure also compares the drag coefficient

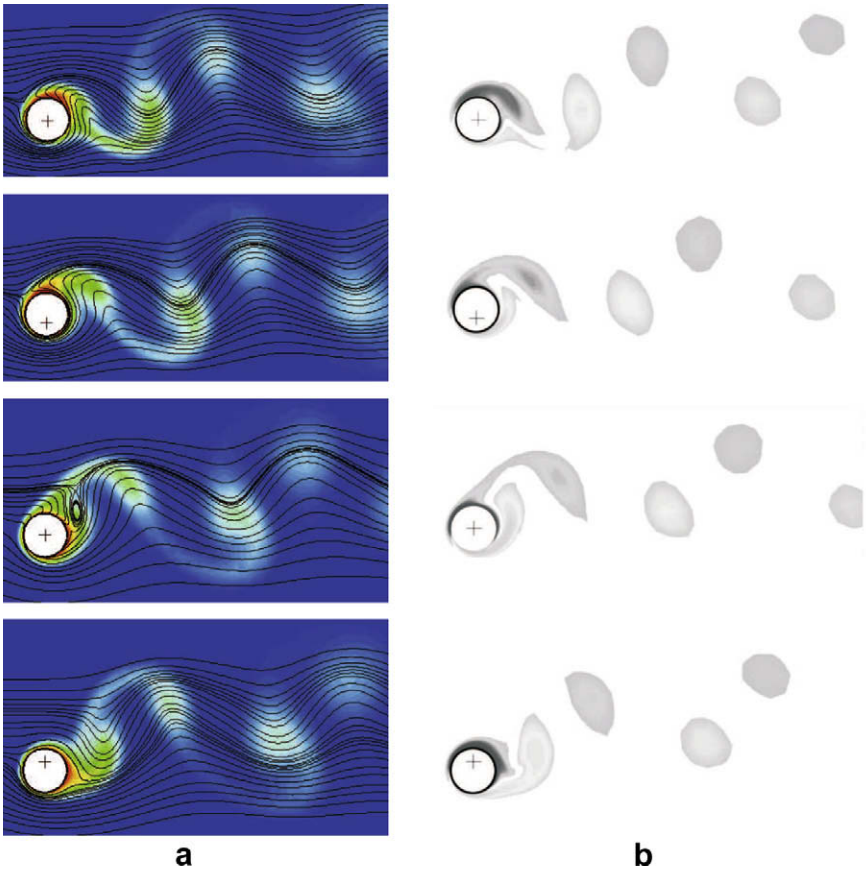

Fig. 9. (a) Temperature field and streamlines, (b) vorticity field for cross-flow oscillating cylinder with rotation at $Re = 100$, $A = 0.2$, $F = 1$, and $\alpha = 1.5$.

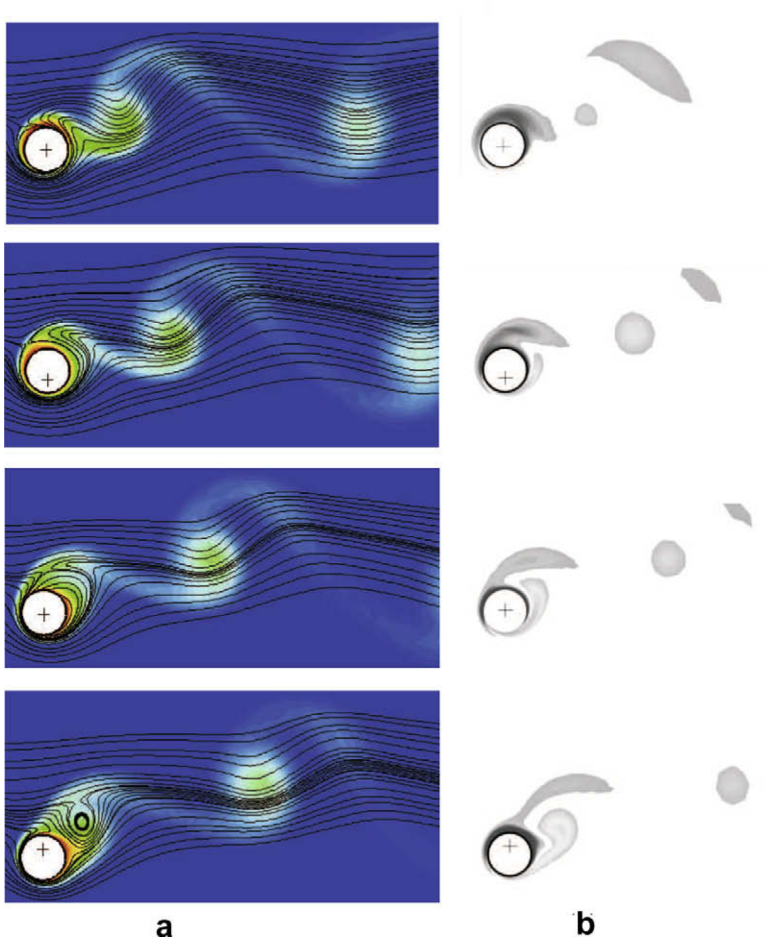

Fig. 10. Streamlines and vorticity field of cross-flow oscillating cylinder for the case of super critical non-dimensional rotational speed, $\alpha = 2.5$, $Re = 100$, $A = 0.2$, and $F = 1$.

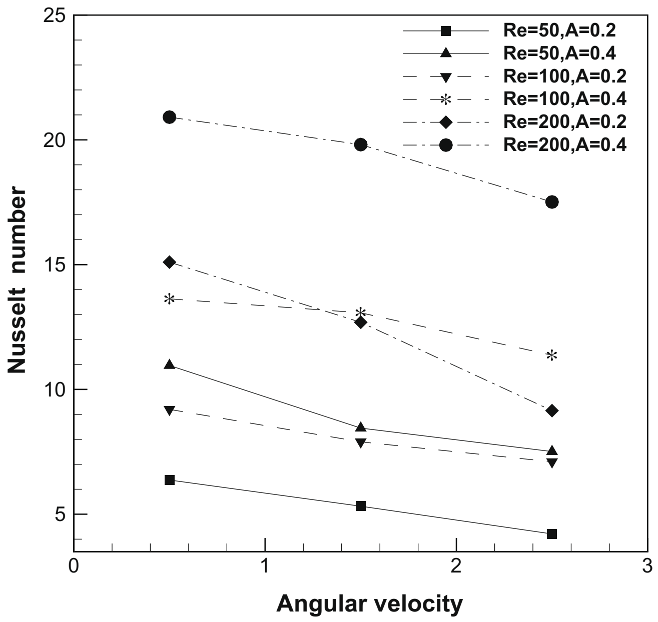

Fig. 11. Variation of mean Nusselt number vs. non-dimensional rotational speed of cross-flow oscillating cylinder at different values of Re and A for $F = 1$.

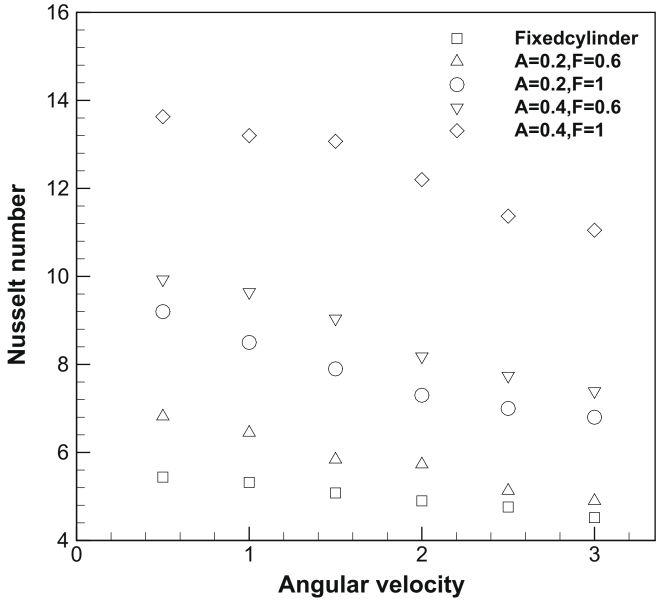

Fig. 12. Variation of mean Nusselt number vs. non-dimensional rotational speed of cross-flow oscillating cylinder and fixed rotating cylinder at different values of A and F for $Re = 100$.

of the oscillating cylinder with the results of the fixed cylinder. At the frequency less than the Strouhal frequency ($F = 0.6$ in the figure), the drag coefficient is nearly the same as the fixed cylinder. However, by increasing the frequency of oscillation up to the

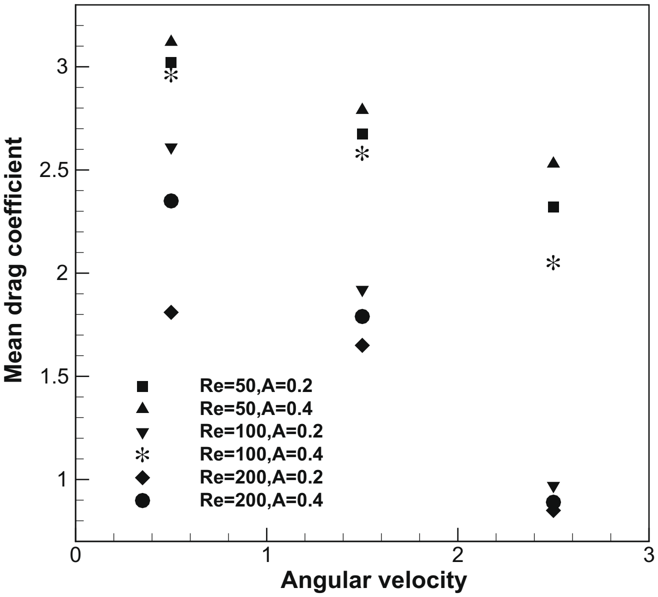

Fig. 13. Variation of mean drag coefficient vs. non-dimensional rotational speed of cross-flow oscillating cylinder at different values of *Re* and *A* for $F = 1$.

Table 2
Mean Nusselt number for cross-flow oscillation at different *Pr* and *A* for $Re = 100$.

α	$Pr = 0.7$	$Pr = 6$	$Pr = 20$
$A = 0.2$			
0.5	9.2	41.3	75.4
1.5	7.9	35.2	70.4
2.5	7.1	25.8	50.7
A=0.4			
0.5	13.6	61.4	105.2
1.5	13.0	55.7	91.4
2.5	11.4	52.2	76.5

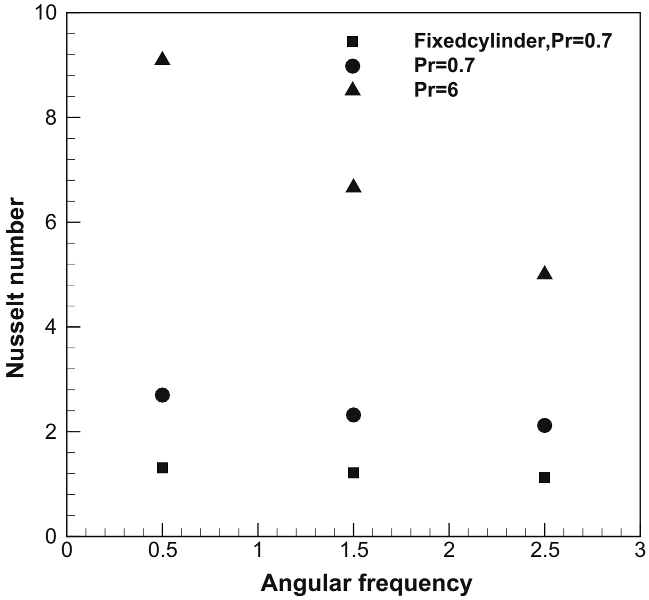

Fig. 14. Variation of mean Nusselt number vs. non-dimensional rotational speed of cross-flow oscillating cylinder at constant heat flux boundary condition for cross-flow oscillating cylinder at different values of *Pr* for $F = 1,\ A = 0.4$, and $Re = 100$.

lock-on occurrence ($F = 1$ in the figure), the drag coefficient increases.

Values of the mean Nusselt number on the cross-flow oscillating cylinder at different Prandtl numbers and amplitudes of oscillation for $Re = 100$ are listed in Table 2. It is seen that by increasing the rotational speed of the cylinder, the Nusselt number decreases. Also increasing the Prandtl number results in the reduction of the thermal boundary-layer thickness causing a large temperature gradient around the cylinder which increases the mean Nusselt number.

For the iso-flux boundary condition, the definition of the local Nusselt number is as follows:

$$Nu_Q = \frac{1}{T_s^* - T_\infty^*}, \tag{23}$$

where T_s^* is the non-dimensional surface temperature and T_∞^* is the non-dimensional free stream temperature. The variation of the mean Nusselt number with respect to the non-dimensional rotational speed of the cylinder corresponding to the constant heat flux boundary condition in the cross-flow oscillating case is shown in Fig. 14 at different values of *Pr* for $F = 1,\ A = 0.4$, and $Re = 100$. Similar trends as explained in the iso-temperature boundary condition are also observed in this case.

6. Conclusions

A numerical study of two-dimensional forced convection over a rotating cylinder with a cross-flow oscillation is carried out using a CBS finite element method to solve the governing equations including continuity, full Navier–Stokes, and energy equations. The CBS scheme is coupled to the dynamic grid using the ALE formulation. The moving grid technique which is based on the modified torsional spring analogy is used to simulate large boundary movements easily.

The variations of the mean Nusselt number, the drag and the lift coefficients with respect to the non-dimensional rotational speed of the cylinder, amplitude and frequency of oscillation, Reynolds number, and Prandtl number are studied in detail. It is found that similar to the fixed cylinder case, a critical non-dimensional rotational speed exists beyond which the vortex shedding is mainly suppressed. The magnitude of critical non-dimensional rotational speed is approximately the same as the fixed cylinder. Also the numerical results obtained indicate that the average Nusselt number fluctuates at twice the cylinder frequency with remarkable enhancement in the heat transfer at high frequencies within the lock-on region. Similar to the velocity field, the thermal field in the wake region is influenced by the vortex shedding process. The vortex lock-on causes the Nusselt number, drag and lift forces to increase dramatically. On the other hand, the drag and the Nusselt number decrease with respect to the angular velocity due to thickening the thermal boundary-layer thickness.

Appendix A

Using the same shape functions for all variables, it can be written

$$U_i = \sum_{a=1}^{3} N^a \overline{U}_i^a, \quad p = \sum_{a=1}^{3} N^a \bar{p}^a, \quad U_i^* = \sum_{a=1}^{3} N^a \overline{U}_i^{*a}, \quad T = \sum_{a=1}^{3} N^a \overline{T}^a, \tag{24}$$

where overline represents the nodal quantities. Eqs. (15)–(18) are now weighted by $\mathbf{N}^T$ and integrated over the entire domain. Applying integration by parts for the viscous terms, the discretized steps of CBS scheme become

$$\mathbf{M}(\overline{\mathbf{U}}^{*} - \overline{\mathbf{U}}^{\mathbf{n}}) = -\Delta \mathbf{t}\left[\mathbf{C_u}\overline{\mathbf{U}} + \mathbf{K}_{\tau\bar{\mathbf{u}}} - \mathbf{f} - \Delta \mathbf{t}(\mathbf{K_u}\overline{\mathbf{U}} - \mathbf{f_s})\right]^{\mathbf{n}}, \tag{25}$$

$$\Delta t\mathbf{H}\bar{\mathbf{p}}^{n+1} = \mathbf{G}\overline{\mathbf{U}}^{*} - \mathbf{f}^{\mathbf{p}}, \tag{26}$$

$$\Delta\overline{\mathbf{U}}_i = \Delta\overline{\mathbf{U}}_i^{*} + \mathbf{M}^{-1}\Delta t\left[\mathbf{G}^T\left(\bar{\mathbf{p}}^{n+1} + \frac{\Delta t}{2}\mathbf{P}\bar{\mathbf{p}}^{n}\right)\right], \tag{27}$$

$$\mathbf{M}(\bar{\mathbf{T}}^{n+1} - \bar{\mathbf{T}}^{n}) = -\Delta t\left[\mathbf{C}_T\bar{\mathbf{T}} + \frac{1}{\rho C_p}(\mathbf{K}_T\overline{T} - \mathbf{f}_e) - \Delta t(\mathbf{K}_u\bar{\mathbf{T}} - \mathbf{f}_{es})\right]^{n}, \tag{28}$$

where the coefficient matrices are defined as

$$\begin{aligned}
&\mathbf{M} = \int_\Omega \mathbf{N}^{\mathbf{T}}\mathbf{N}\,d\Omega, \quad \mathbf{C}_u = \mathbf{C}_T = \int_\Omega \mathbf{N}^T\frac{\partial(u_i\mathbf{N})}{\partial x_i}d\Omega,\\
&\mathbf{K}_\tau = \int_\Omega \frac{\partial \mathbf{N}^T}{\partial x_i}\nu\frac{\partial \mathbf{N}}{\partial x_i}d\Omega, \quad \mathbf{f} = \int_\Omega \mathbf{N}^T Q\,d\Omega + b.t.\\
&\mathbf{G} = \int_\Omega \frac{\partial \mathbf{N}^T}{\partial x_i}\mathbf{N}\,d\Omega, \quad \mathbf{H} = \int_\Omega \frac{\partial \mathbf{N}^T}{\partial x_i}\frac{\partial \mathbf{N}}{\partial x_i}d\Omega,\\
&\mathbf{f}^p = \Delta t\int_\Gamma \mathbf{N}^T n^T\left[\bar{\mathbf{U}}^n - \Delta t\nabla p^{n+1}\right]d\Gamma,\\
&\mathbf{f}_e = \int_\Gamma \mathbf{N}^T n^T k\nabla T\,d\Gamma,\\
&\mathbf{P} = \int_\Omega \frac{\partial}{\partial x_i}\mathbf{N}^t u_i\frac{\partial \mathbf{N}}{\partial x_j}d\Omega, \quad \mathbf{K}_T = \int_\Omega \frac{\partial \mathbf{N}^T}{\partial x_i}k\frac{\partial \mathbf{N}}{\partial x_i}d\Omega,
\end{aligned} \tag{29}$$

where b.t. stands for integrals along region boundaries. Stabilizing matrices are

$$\begin{aligned}
&\mathbf{K}_u = -\frac{1}{2}\int_\Omega \frac{\partial}{\partial x_i}(u_i\mathbf{N}^T)\frac{\partial}{\partial x_i}(u_i\mathbf{N})d\Omega,\\
&\mathbf{f}_s = -\frac{1}{2}\int_\Omega \frac{\partial}{\partial x_i}(u_i\mathbf{N}^T)Q\,d\Omega.
\end{aligned} \tag{30}$$

References

[1] J.H. Gerrard, The mechanics of the formation region of the vortices behind bluff bodies, J. Fluid Mech. 25 (1966) 401–413.

[2] G.H. Koopman, The vortex wakes of the vibrating cylinders at low Reynolds numbers, J. Fluid Mech. 28 (1967) 501–512.

[3] O.M. Griffin, S.E. Ramberg, Vortex shedding from a circular cylinder vibrating inline with an incident uniform flow, J. Fluid Mech. 75 (1976) 257–276.

[4] C.H.K. Williamson, A. Roshko, Vortex formation in the wake of an oscillating cylinder, J. Fluid Struct. 2 (1988) 355–381.

[5] M.S. Hall, O.M. Griffin, Vortex shedding and lock-on in a perturbed flow, Trans. ASME, J. Fluids Eng. 115 (1993) 283–291.

[6] M.R.H. Nobari, H. Naderan, A numerical study of flow past a cylinder with cross flow and inline oscillation, Comput. Fluids 35 (2006) 393–422.

[7] J.R. Filler, P.L. Marston, W.C. Mih, Response of the shear layers separating from a circular cylinder to small-amplitude rotational oscillations, J. Fluid Mech. 231 (1991) 481–499.

[8] S. Baek, H.G. Sung, Numerical simulation of the flow behind a rotary oscillating circular cylinder, Phys. Fluids 10 (1998) 869–876.

[9] F.M. Mahfouz, H.M. Badr, Forced convection from a rotationally oscillating cylinder placed in a uniform stream, Int. J. Heat Mass transfer 43 (2000) 3093–3104.

[10] Wu-Shung Fu, Bao-Hong Tong, Numerical investigation of heat transfer from a heated oscillating cylinder in a cross flow, Int. J. Heat Mass transfer 45 (2002) 3033–3043.

[11] Wu-Shung Fu, Bao-Hong Tong, Effects of eccentricity of cylinder and blockage ratio on heat transfer by an oscillating cylinder in a channel flow, Int. Commun. Heat Mass transfer 30 (2003) 401–412.

[12] S. Kang, H. Choi, S. Lee, Laminar flow past a rotating circular cylinder, Phys. Fluids 11 (1999) 3312–3321.

[13] D.B. Ingham, T. Tang, A numerical investigation into the steady flow past a rotating circular cylinder at low and intermediate Reynolds numbers, J. Comput. Phys. 87 (1990) 91–107.

[14] H.M. Badr, S.C.R. Dennis, P.J.S.J. Young, Steady and unsteady flow past a rotating circular cylinder at low Reynolds numbers, J. Comput. Phys. 17 (1989) 579–609.

[15] T. Tang, D.B. Ingham, On steady flow past a rotating circular cylinder at Reynolds numbers 60 and 100, Comput. Fluids 19 (1991) 217–230.

[16] B. Koobus, C. Farhat, Second-order time-accurate and geometrically conservative implicit scheme for flow computations on unstructured dynamic meshes, Comput. Meth. Appl. Mech. Eng. 170 (1999) 103–129.

[17] P. Nithiarasu, An arbitrary Lagrangian Eulerian (ALE) formulation for free surface flows using the characteristic-based split (CBS) scheme, Int. J. Numer. Meth. Fluids 48 (2005) 1415–1428.

[18] C. Farhat, C. Degand, B. Koobus, M. Lesoinne, Torsional springs for two-dimensional dynamic unstructured fluid meshes, Comput. Meth. Appl. Mech. Eng. 163 (1998) 231–245.

[19] J.A. Chorin, Numerical solution of the Navier–Stokes equations, Math. Comput. 22 (1968) 745–762.

[20] O.C. Zienkiewicz, R. Codina, A general algorithm for compressible and incompressible flow – part I. The split characteristic based scheme, Int. J. Numer. Meth. Fluids 20 (1996) 869–885.

[21] P. Nithiarasu, R. Codina, O.C. Zienkiewicz, The characteristic-based split (CBS) scheme: a unified approach to fluid dynamics, Int. J. Numer. Meth. Eng. 66 (2006) 1514–1546.

[22] O.C. Zienkiewicz, R.L. Taylor, P. Nithiarasu, The Finite Element Method, vol. 3, Fluid Mechanics, sixth ed., Butterworth–Heinemann, Oxford, 2005.

[23] A. Roshko, On the drag and shedding frequency of two-dimensional bluff bodies, Technical Note 3165, National Advisory Committee on Aeronautics (currently NASA), Washington, DC, USA, 1954.

[24] F.P. Incropera, Fundamentals of Heat and Mass Transfer, fifth ed., Wiley, New York, 2002.